2019 2nd IEEE International Conference on Soft Robotics (RoboSoft)
COEX, Seoul, Korea, April 14-18, 2019

A Soft Actuator with Tunable Mechanical Configurations for Object Grasping Based on Sensory Feedback

Xi Fang[1], Zemin Liu[1], Yufei Hao[1], Hui Yang[1], Jiaqi Liu[1], Zhexin Xie[1] and Li Wen[1,2]*, *Member, IEEE*

***Abstract*— In this paper, we propose a soft actuator embedded with conductive liquid alloy (eGaIn) and Shape Memory Polymer (SMP). The conductive liquid alloy functions as bending sensor as well as pressure sensor. The three segments of the SMP layer can be heated optionally by applying 400mA current to different sections of the conductive silver fiber to achieve tunable stiffness, and enable the soft actuator with variable degree-of-freedom (DoF) configurations. Through real-time feedback of the bending sensor that has been calibrated, we realized proprioception of all mechanical configurations of the soft actuator under free load. We also achieved geometrical feature recognition of different objects while all segments of the actuator were softened. Finally, experimental verification of the prototype was conducted on a variety of objects in condition that the geometrical features were unknown. The results show improved enveloping and reliable grasping performance.**

I. Introduction

Soft robots generally have a continuously deformed structure with kinematic redundancy [1]. Relying on different properties of constituent materials, soft robots can achieve high curvature bending and large torsion, and can absorb energy during collision [2]. Soft robots can also work in a confined space, such as the minimally invasive surgery [3]. Its strong adaptability and high sensitivity are beyond traditional rigid robots. Soft robots are usually driven by hydraulic/ pneumatic pressure [4]-[6], cables [7], chemical energy [8] and smart materials [9]-[10], to mimic the biological muscles and achieve various movements. However, the low rigidity of soft robots induces monotonous motion patterns, and the large deformation brings challenges to sensory feedback and control of soft robots. Therefore, it is difficult for a soft gripper to achieve an programmable envelop and grasping on objects with different morphological structures.

A few studies have investigated approaches to tune the material stiffness thus to change the low rigidity of soft robots. Some study embedded rigid materials into soft materials such as Low-Melting-Point Alloy (LMPA) [11]-[12], wax [13], etc. Some other work achieved different motions by changing morphological origami structures off-line [14]. To implement a soft actuator that has multiple DoF configurations, researchers embedded functional materials with variable stiffness into the body or joints of the actuator, such as

This research was supported by the National Science Foundation key project, China under contract number 61633004 and the National Science Foundation project for Excellent Young Scholar, China under contract number 61822303. Authors are with the School of Mechanical Engineering and Automation[1], and Beijing Advanced Innovation Center for Biomedical Engineering[2], Beihang University, Beijing, 100191, People's Republic of China. *Author for correspondence. (Prof. Li Wen, liwen@buaa.edu.cn)

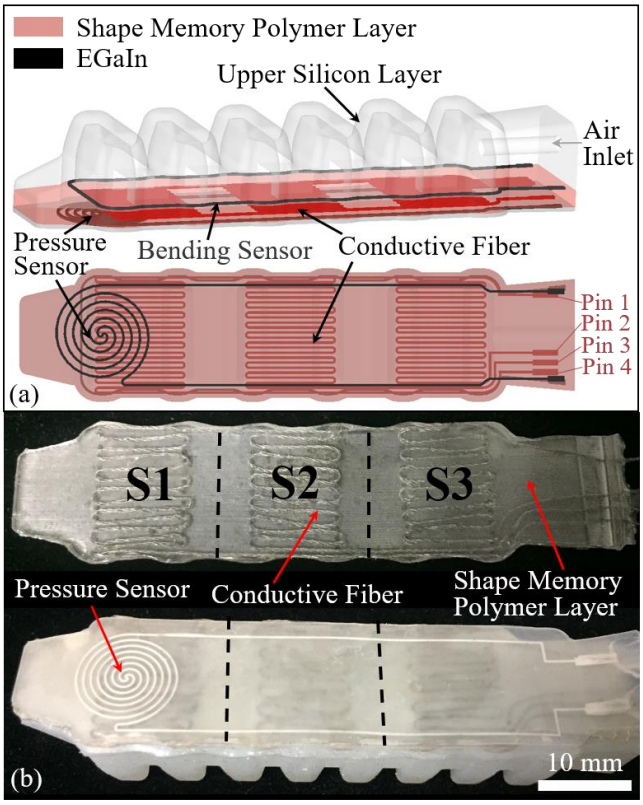

Figure 1. The prototype design of the soft actuator with multiple DoF configurations and variable stiffness. (a) The whole model (upper) and the bottom view (down). The bending sensor was embedded into the upper silicon layer to obtain curvature feedback in the real-time control. The conductive fiber serves as heat source of SMP layer to achieve variable stiffness. By applying a current to different sets of pin 1~4, corresponding sections of the SMP layer will be heated. The pressure sensor was put underneath the gripper to perceive contact information when grasping. (b) The SMP layer (upper) and bottom view of the prototype (down). The conductive silver yarn was embedded into the SMP layer during fabrication to accelerate the heating process.

conductive propylene-based elastomer [15], LMPA [16] and SMP [17]-[18]. Although the previous methods have contributed to tunable stiffness and improved the low rigidity of soft robots, the multiple DoF configurations with piecewise compliance is still a great challenge.

Recently, flexible sensors, such as optoelectronic strain sensors [19] and carbon doped PDMS sensors [20], have been integrated into soft actuators. EGaIn is also an ideal sensor for soft actuators due to its liquid state at room temperature, high ductile performance and high conductivity. eGaIn has been used for curvature sensing, exteroceptive contact sensing and inflation sensing [21], as well as strain perception [22], shear force sensing [23] and flexible electric wire [24]. Except for sensory feedback, the nonlinear deformation also brings

challenges to the control of soft robots. Researchers proposed Piecewise Constant Curvature (PCC) model for continuously deformed soft robots [25], and combined it with PID feedback control [26], which has obtained improved controlling performance.

In this paper, we propose a soft actuator embedded with conductive liquid alloy (eGaIn) and SMP, which has variable stiffness and multiple DoF configurations. The eGaIn functions as bending sensor and pressure sensor. Multiple DoF configurations with piecewise compliance can be achieved by selectively heating different segments of the SMP layer. The conductive silver fiber was embedded in the SMP layer to accelerate the heating process. Different functional layers were fabricated separately and bonded together to form the prototype. Through real-time feedback of the bending and pressure sensors, proprioception and exteroception (i.e., geometrical feature recognition of the object) are realized. Experiments were carried out to test the bending and force responses of the sensors. Based on the shape recognition result, the gripper was reconfigured to achieve improved envelop on the object. The grasping verification was then conducted in condition that the object shape is unknown.

II. Materials and Methods

A. Design and Fabrication of the Prototype

The prototype design of the soft actuator is shown in Figure 1. The structure is composed of three layers: the upper silicon layer embedded with bending sensor, the middle SMP layer embedded with conductive silver fabric and the bottom layer of pressure sensor. The bending sensor was to obtain curvature feedback in the real-time control. The conductive fiber serves as heat source of SMP layer to achieve variable stiffness. The spiral pressure sensor was put underneath the gripper to perceive contact information [27] when grasping. As Figure 1(a) demonstrates, by applying 400mA current to different sets of pin 1~4, different segments of the SMP layer will be heated and the SMP layer can be softened within 1.2s. The heating laws are shown in TABLE I. Note that the pin numbers can be found in Figure 1(a). At room temperature, the unheated parts of SMP layer remain rigid and the corresponding segments of the gripper can hardly bend even under pneumatic actuation.

For accurate sensory feedback, microchannel with a cross section of 0.3mm in length and 0.3mm in width was fabricated with silicon rubber Dragon Skin 20 (Smooth-on Inc., USA) in the way described in [27]. Then the conductive liquid alloy eGaIn (Sigma-Aldrich Inc., USA) was infused into the microchannel using two syringes [27]. To fabricate the SMP layer, two compounds named EPON 828 and Jeffamine D400 were mixed in weight proportion 25:9 [30]. After 24-hour

TABLE I. Heating Laws of the Soft Actuator

Pin		Heated Sections	Dof Configuration	Pin		Heated Sections	Dof Configuration
1	2	S3		2	4	S1, S3	
1	3	S2		3	4	S1, S2	Mode 2
1	4	S1	Mode 1	2(+), 3(-), 4(-)		S1, S2, S3	Mode 3
2	3	S2, S3					

standing at 25℃, the mixture was poured into the mold and heated at 70℃ for six hours. Finally, in order to embed the heating layer into the SMP layer to achieve better heating efficiency, the uncured mixture was poured over the silver fabric (0.3mm in diameter) and let it stand still for 24 hours at 25℃. Furthermore, the glass transition temperature of the SMP layer is 44.0±0.6℃ [28], which means that the stiffness can be easily and quickly changed under heating. The upper silicon structure was also made of Dragon Skin 20, and was fabricated with molding process. Finally, all the parts were fitted together using QIS-3009 (DongGuan JingDa Adhesive Co., Ltd China).

B. Characteristics of Bending and Pressure Sensors

In order to measure the properties of the bending sensor and the pressure sensor, four experiments were conducted to calibrate the characteristics and test the air pressure and force response performances of the sensors.

The first experiment was to calibrate the relative resistance variation characteristics of the bending sensor under four different DoF configurations. To measure the resistance of the bending sensor, a steady current of 10mA was applied to the sensor. The air pressure input increased from 3kPa to 60kPa with an interval of 3kPa. As Figure 2 shows, the PC sent digital pressure control command to the board at a regular interval, and then the pneumatic control unit received voltage signals from the board to actuate the soft actuator. The voltage data was recorded on the PC. Three experiments were implemented, and the average relative resistance variations were acquired.

The second experiment was conducted to obtain the relative resistance variation characteristics of the pressure sensor when the condensing force applied to the sensor increases. The calibration was conducted within the range of pressure sensor, and the maximum force could meet the requirements of subsequent grasping experiments. In Figure 5(b), the six-axis force transducer (Mini 40 F/T sensor, ATI, USA) was mounted on the tip of the robotic arm (MOTOMAN MH3F, YASKAWA Inc., Japan), and the pressure sensor was connected to a digital multimeter (Fluke 8845A, Fluke Inc., USA). The robotic arm moved downwards at 0.3mm/s, with a total displacement of 0.3mm and a step of 0.03mm. Note that there is a four-second interval between each step. During the experiment, the force data was recorded on the PC, and the resistance data was recorded in a NI data acquisition board

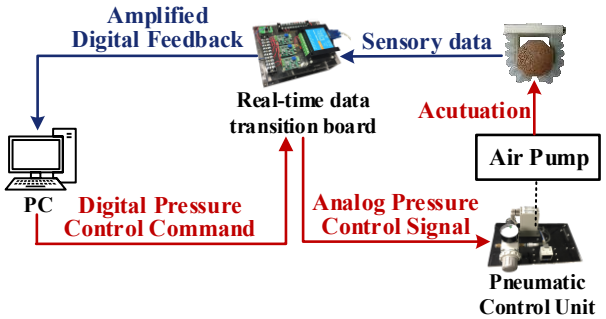

Figure 2. Pneumatic control system for the soft actuator on which most of the experiments were carried out. The pneumatic control unit is composed of proportional air valves (ITV0030, SMC, Japan), air pressure sensors (ISE30A-01-C, SMC, Japan) and a pressure gauge.

(PCI-6284, National Instruments, USA) at the same time.

The third and fourth experiments were performed to test pressure and force responses of the bending sensor and the pressure sensor, using the pneumatic control system shown in Figure 2. In Figure 5(c), PC sent the saw tooth wave signal of air pressure to the board at 25Hz. Meanwhile the board collected the voltage data of the sensor at 25Hz. In Figure 5(d), the robotic arm moved downwards at 4mm/s with a total displacement of 0.4mm. The condensing force was measured by the six-axis force transducer and recorded by the NI data acquisition board. The voltage data of the sensor was recorded by the real-time data transition board at 25Hz.

C. *Model-based Object Grasping*

Figure 3 demonstrates the process of improved grasping of different objects in condition that the geometrical features of the object is unknown. The first step is to configure the gripper in fully softened state and envelop the object. By prebuilding a point set $O_{shape}(x,y)$, where x and y represent sensory data collected by the bending sensor and the pressure sensor after enveloping, the shape of the object can be predicted. Then the DoF configuration for improved grasping is selected by experience. Finally, an effective grasp is conducted on the object by controlling the soft actuator in closed loop. Note that l_k is the length of each segment. The whole procedure is also demonstrated in the supplementary video in detail.

PCC kinematics model [25] in Figure 4(a) was utilized for the closed-loop control. There are some assumptions as follows to simplify the control. ①The heated segments bend in a constant curvature. On the contrary, the unheated segments remain straight. ② The bending segments keep tangent to the rigid segments under inflection. ③The length of the actuator keeps constant during inflection, i.e., leaving out axial deformation.

As Figure 4(b) reveals, the gripper was fastened to a base. Take the condition in Figure 4(a) as an example: the tip and middle segments are softened while the root segment remains rigid. Equation (1) can be deduced from the geometrical relationship in Figure 4(a), where l is the length of each segment, θ is the angle between axis y_1 and o_1o_3, and r is the radius of the bending segments. According to [25], in equation (2), the transformations from the coordinate system $o-x_0y_0z_0$ to $o-x_3y_3z_3$ include two translations and a rotation around axis z by θ. Once target coordinate of the tip (x_{target}, y_{target}) is determined, we can obtain the curvature κ of the bending segments in equation (3). For other DoF configurations, similar conclusion can be deduced by changing the value of l.

$$d = \frac{2l\sin\theta}{\theta},\ \theta = \frac{l}{r} \tag{1}$$

$${}^{3}_{0}T = \begin{bmatrix} \cos\frac{2l}{r} & \sin\frac{2l}{r} & 0 & 2\sin^2\frac{l}{r} \\ -\sin\frac{2l}{r} & \cos\frac{2l}{r} & 0 & l+2r\sin\frac{l}{r} \\ 0 & 0 & 1 & 0 \\ 0 & 0 & 0 & 1 \end{bmatrix} \tag{2}$$

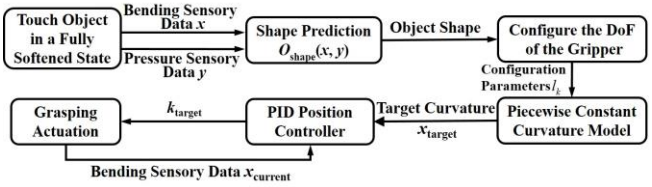

Figure 3. Flow diagram of model-based object grasping under the condition of unknown shape of the object.

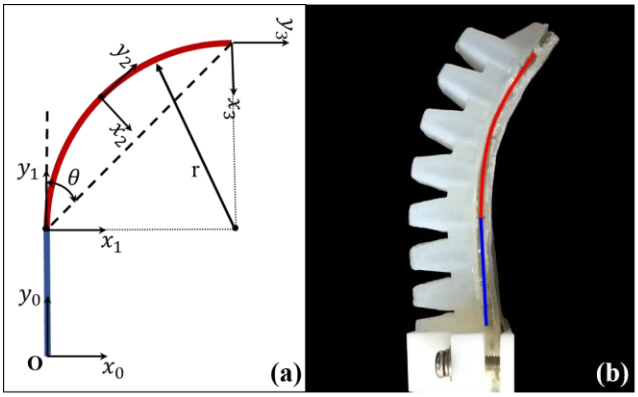

Figure 4. Kinematics model of the gripper. (a) PCC kinematics model of the gripper. (b) Corresponding DoF configuration of the prototype.

$$\kappa = \frac{1}{l}\arcsin\sqrt{\frac{x_{target}}{2}} \tag{3}$$

Once the object shape is predicted, the inverse kinematics model mentioned above can be used for closed-loop control. After inputting a target for the curvature controller, the curvature error $e_k = x_{target} - x_{current}$ is calculated for PID feedback control in equation (4), where $x_{current}$ is obtained from the feedback of bending sensor. In case of suppressing periodic interference and random disturbances, a mean filter is employed to smooth the sensory data by averaging three contiguous values.

$$k_{target} = K_p e_k + K_i \int e_k dt + K_d \dot{e}_k \tag{4}$$

D. *Real-time control system for the actuator with sensory feedback*

A pneumatic control system shown in Figure 2 was designed for controlling the motion of the soft actuator. The real-time data transition board can collect the sensory data and return amplified signals to the PC at 100Hz maximally. It can also send the pressure control command from the PC to the pneumatic control unit. During the experiments, all data are processed and recorded on the PC.

III. RESULTS

A. *Characteristics of the Sensors and Geometrical Feature Recognition*

The calibration results of the bending sensor are demonstrated in Figure 5(a). Due to the nonlinear relationship between curvature of the soft actuator and change of air pressure, the relative resistance varies with the air pressure in a nonlinear way. For the three different DoF configurations, correlation coefficients were obtained by fitting the relationships between air pressure and relative resistance with

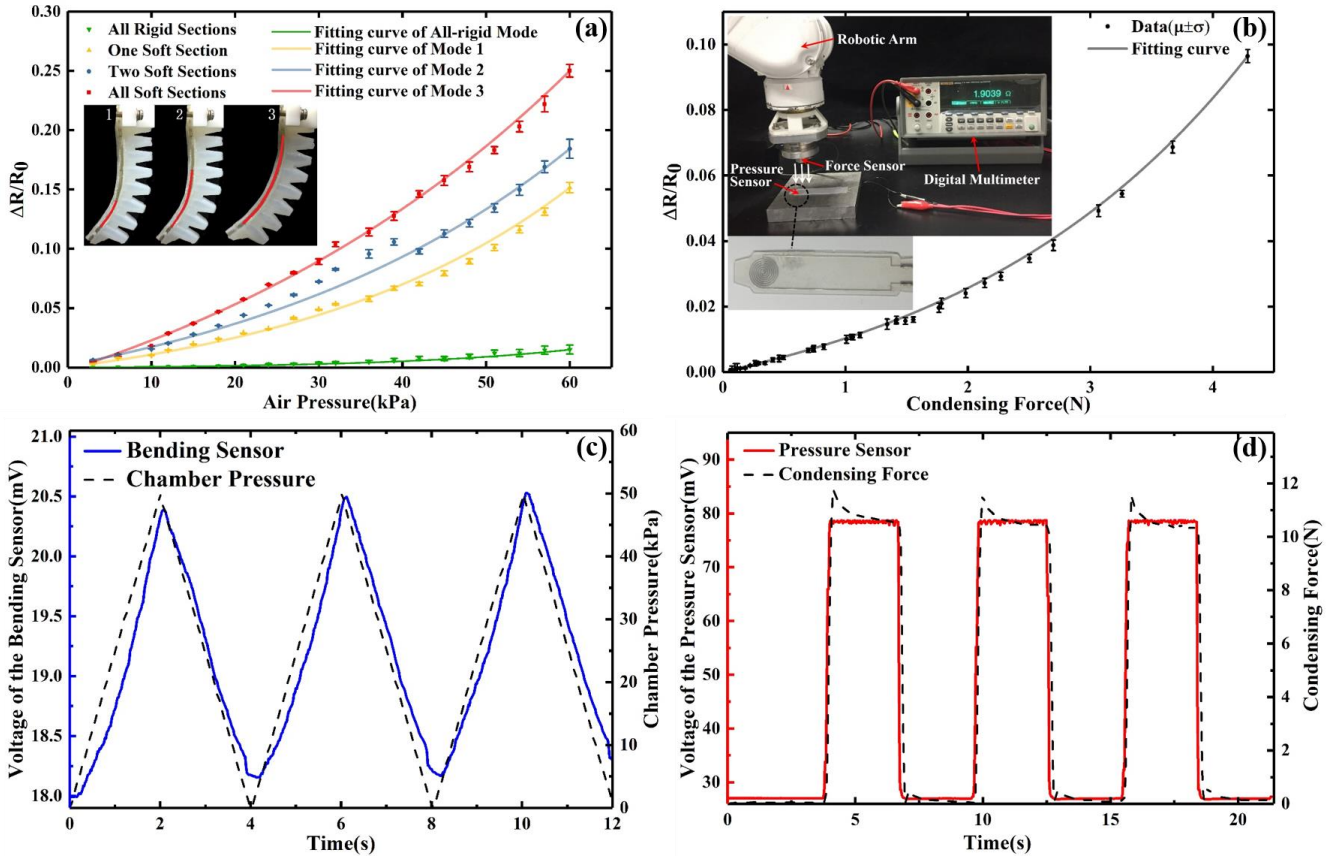

Figure 5. The characteristics and pressure/force responses of the sensors. (a) Relative resistance variations of the bending sensor as a function of the chamber pressure. For Mode 1, Mode 2 and Mode 3, the red-marked sections of the gripper represent heated segments with bending capacity. (b) Relative resistance variation of the pressure sensor with increase of the condensing force applied to the sensor, and the experimental setup of testing characteristics of the pressure sensor (upper left). (c) Chamber pressure response of the bending sensor. The dotted line shows the change of chamber pressure, while the solid line represents the voltage variation of the bending sensor over time. (d) Force response of the pressure sensor. The dotted line shows the change of condensing force applied to the sensor, while the solid line represents the voltage variation of the pressure sensor over time.

quadratic curves. The functions for the fitted curves are as follows (for Mode 1, Mode 2, Mode 3 respectively),

$$\begin{cases} y_1 = 0.0001x^2 + 0.0061x \ (R^2 = 0.9975) \\ y_2 = 0.0001x^2 + 0.0044x \ (R^2 = 0.9970) \\ y_3 = 0.00009x^2 + 0.0019x \ (R^2 = 0.9895) \end{cases} \quad (5)$$

Compared to Mode 1 and Mode 2, the gripper working in Mode 3 causes maximum deformation of the bending sensor, therefore resulting in greatest relative resistance variation when air pressure increases. For the all-rigid mode, the relative resistance barely changes with air pressure increasing, which means puny deformation of rigid segments in real-time control. Besides, minimum variation of 0.00318 was detected on the relative resistance when the air pressure was 3kPa, which we approximate as the resolution of bending sensor.

Figure 5(b) shows the calibration results of pressure sensor. Because of the nonlinear deformation of the pressure sensor, the relative resistance grows with the condensing force applied to the tip of the actuator in a nonlinear way. Sensory data were fitted with a quadratic curve that has a good correlation coefficient. The function of the fitted curve is as follows.

$$y_4 = 0.015x^2 + 0.0186x \ (R^2 = 0.9955) \quad (6)$$

In Figure 5(c)-(d), pressure and force responses, repeatability and stability of the sensors were tested. Result of the bending sensor reveals that it can provide real-time feedback of repeated signals with little delay (0.1s approximately), which is very important for grasping control. Result of the pressure sensor indicates that it can respond to periodic signals in a quick and steady way.

After that, a clustered point set which is essential for the subsequent geometrical feature recognition is pre-established. As shown in Figure 6, after enveloping grasps on different shapes of objects, the sensory data shows clustered distribution, which once again proves that the repeatability and stability of the sensors. For objects with different shapes, the sensory data are independent without overlap, which contributes to improving confidence of the shape prediction. The results show that bending sensor can reproduce the contours and size of the object, while pressure sensor can reproduce contact force. Compared with smooth ball, the spiny ball has the same diameter but different roughness, which causes similar bending sensory data but higher pressure sensory data. What's more, bending sensory data indicates that the octagonal prism and the cuboid have contours with highest curvatures; pressure sensory data indicates that the gripper detected greatest contact force on octagonal prism. For the size of each tested object refer to Figure 8. Note that all tests are under the same air pressure input.

In Figure 6, ten grasps were performed for each object, from which average and standard deviation of the sensory data were obtained. Fitting area of the point set for each specific

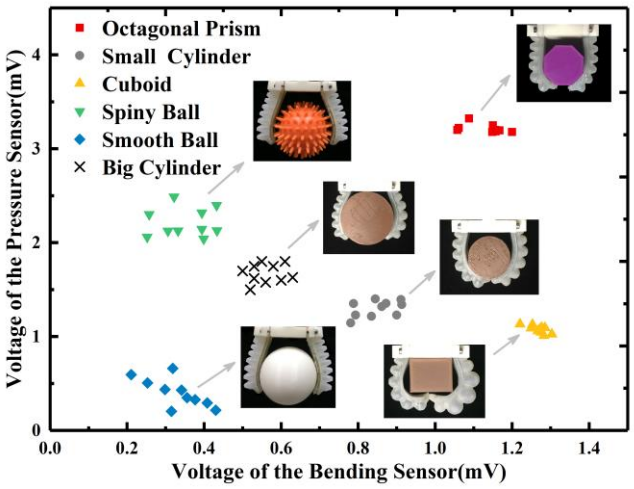

Figure 6. Clustered sensory data for enveloping grasps. Ten grasps were conducted for each object. The gripper was fully softened during the experiment. See supplementary video for more details.

TABLE II. SHAPE PREDICTION AND GRASPING CONFIGURATION

Type	Comparison		DoF Configuration
	Pre-build set	*Recognition Result*	
Cuboid	$(x-1.27)^2+(y-1.08)^2 \le 0.045^2$	(1.29, 1.11)	Mode 1
Octagonal Prism	$(x-1.13)^2+(y-3.21)^2 \le 0.062^2$	(1.15, 3.16)	Mode 1
Small Cylinder	$(x-0.85)^2+(y-1.30)^2 \le 0.095^2$	(0.77, 1.25)	Mode 2
Big Cylinder	$(x-0.56)^2+(y-1.67)^2 \le 0.105^2$	(0.63, 1.73)	Mode 3
Smooth Ball	$(x-0.33)^2+(y-0.40)^2 \le 0.159^2$	(0.27, 0.51)	Mode 3
Spiny Ball	$(x-0.35)^2+(y-2.21)^2 \le 0.158^2$	(0.28, 2.12)	Mode 3

Physical unit (mV). For Mode 1-3, refer to TABLE I.

object was obtained in equation (7), where the average (x_0, y_0) was regarded as the center coordinate of the circle, and the standard deviation σ was regarded as the radius of the circle.

$$O_{shape}(x,y):\ (x-x_0)^2+(y-y_0)^2 \le \sigma^2 \tag{7}$$

In the process of shape prediction, the soft gripper enveloped the object with unknown shape in a completely softened state, and the sensory data was collected three times and then averaged. The experimental results in TABLE II show that enveloping of each object with unknown shape is effective. The sensory feedback reveals that the object is within the range of the pre-established point set, which brings about relatively high recognition confidence.

B. Closed-loop Control Results of the Soft Gripper

Figure 7 shows the closed-loop PID control results of different DoF configurations under free load. The parameters K_p, K_i, K_d for PID position control were set to 0.984, 0.011, 0 respectively after regulation. For each configuration, the difference between simulation and experimental results grows slightly with air pressure, because the rigid segments deform mildly under inflation. As the inflation pressure increases, the deformation of the rigid segments increases, causing the root of the soft gripper to be not perpendicular to the horizontal plane of the base. However, the control error is within

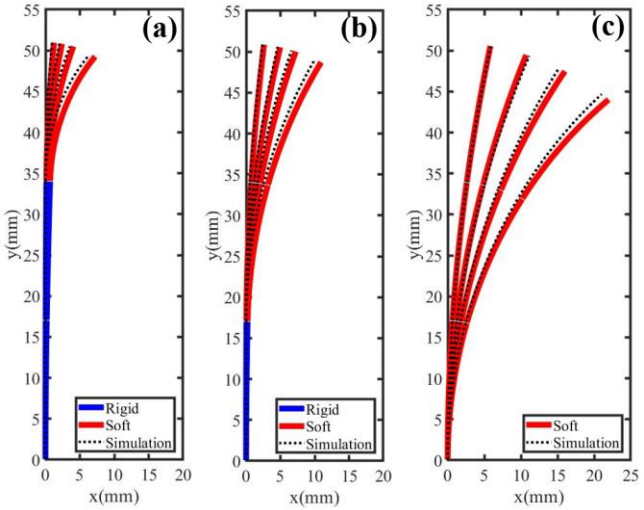

Figure 7. Comparisons between experimental results and model-based simulations of closed-loop control of the soft gripper under different DoF configurations.

allowable range. Moreover, the error does not have a great impact on the grasp of objects, because it enables the soft gripper to apply a larger enveloping force to grasp, which increases the reliability of grasping to a certain extent.

C. Grasping Verification Experiments

Figure 8 presents the results of grasping verification. Four shapes were tested in this experiment. After shape prediction, a specific DoF configuration was chosen for grasping the object, shown in TABLE II. In Figure 8(a)-(b), the tip segment was softened to grasp a cuboid or an octagonal prism. In Figure 8(c), the tip and middle segments were softened for grasping a small cylinder. In Figure 8(d), all segments of the gripper were softened for enveloping a large cylinder. The

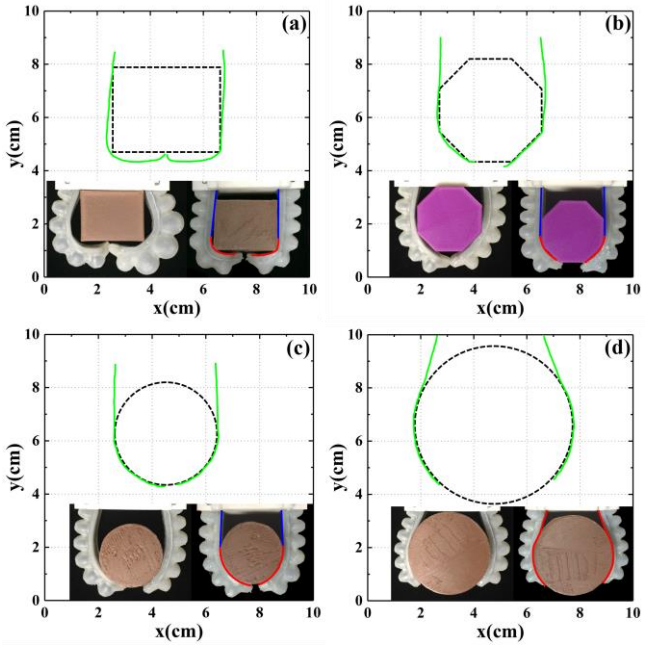

Figure 8. Grasping Verifications of objects with different shapes. In each subgraph, the picture at bottom left shows the enveloping result of the gripper in a fully softened state, while the picture at bottom right represents the improved enveloping performance of the gripper under a specific DoF configuration.

results reveal that by adopting different DoF configurations, we achieved improved enveloping of different objects compared to actuating the soft gripper in a fully softened way.

IV. Conclusion and Discussion

In this paper, we propose a soft actuator that achieves multiple DoF configurations and piecewise compliance, which contributes to geometrical feature recognition and improved enveloping of objects with unknown shapes. The three segments of the SMP layer can be selectively heated to achieve tunable stiffness and different motion configurations. The embedded conductive liquid alloy functions as bending sensor as well as pressure sensor, which show good repeatability, stability and robustness. Through real-time feedback of the sensors, proprioception and exteroception (i.e., geometrical feature recognition) are realized. Finally, the grasping verification was conducted on objects with different shapes, which shows improved enveloping and reliable grasping performance.

In the future, precise shape perception and grasping strategy for enveloping objects with unknown shapes worth further efforts. Future work includes integrating more sensors to enhance the perception and control ability of the soft actuator and exploring efficient and reliable grasping strategies, as well as employing machine learning to improve sensory analysis.

Appendix

See the supplementary video for more details.

Acknowledgment

Thanks Lei Li for his kind help on the experimental setup.

References

[1] Rolf M, Steil J J. "Constant curvature continuum kinematics as fast approximate model for the Bionic Handling Assistant", in *Intelligent Robots and Systems (IROS), 2012 IEEE/RSJ International Conference on. IEEE*, 2012, pp. 3440-3446.

[2] Seok S, Onal C D, Cho K J, et al. "Meshworm: a peristaltic soft robot with antagonistic nickel titanium coil actuators", *IEEE/ASME Transactions on mechatronics*, 2013, vol 18, no 5, pp. 1485-1497.

[3] Ranzani T, Gerboni G, Cianchetti M, et al. "A bioinspired soft manipulator for minimally invasive surgery", *Bioinspiration & biomimetics*, 2015, vol 10, no 3, pp. 035008.

[4] Marchese A D, Rus D. "Design, kinematics, and control of a soft spatial fluidic elastomer manipulator", *The International Journal of Robotics Research*, 2016, vol 35, no 7, pp. 840-869.

[5] Martinez R V, Branch J L, Fish C R, et al. "Robotic tentacles with three - dimensional mobility based on flexible elastomers", *Advanced materials*, 2013, vol 25, no 2, pp. 205-212.

[6] Polygerinos P, Wang Z, Galloway K C, et al. "Soft robotic glove for combined assistance and at-home rehabilitation", *Robotics and Autonomous Systems*, 2015, vol 73, pp. 135-143.

[7] Manti M, Hassan T, Passetti G, et al. "A bioinspired soft robotic gripper for adaptable and effective grasping", *Soft Robotics*, 2015, vol 2, no 3, pp. 107-116.

[8] Wehner M, Truby R L, Fitzgerald D J, et al. "An integrated design and fabrication strategy for entirely soft, autonomous robots", *Nature*, 2016, vol 536, no 7617, pp. 451.

[9] Laschi C, Cianchetti M, Mazzolai B, et al. "Soft robot arm inspired by the octopus", *Advanced Robotics*, 2012, vol 26, no 7, pp. 709-727.

[10] Hao Y, Wang T, Xie Z, et al. "A eutectic-alloy-infused soft actuator with sensing, tunable degrees of freedom, and stiffness properties", *Journal of Micromechanics and Microengineering*, 2018, vol 28, no 2, pp. 024004.

[11] Shan W, Lu T, Majidi C. "Soft-matter composites with electrically tunable elastic rigidity", *Smart Materials and Structures*, 2013, vol 22, no 8, pp. 085005.

[12] Yufei H, Tianmiao W, Xi F, et al. "A variable stiffness soft robotic gripper with low-melting-point alloy", in *Control Conference (CCC), 2017 36th Chinese. IEEE*, 2017, pp. 6781-6786.

[13] Cheng N G, Gopinath A, Wang L, et al. "Thermally Tunable, Self-Healing Composites for Soft Robotic Applications", *Macromolecular Materials and Engineering*, 2014, vol 299, no 11, pp. 1279-1284.

[14] Martinez R V, Fish C R, Chen X, et al. "Elastomeric origami: programmable paper - elastomer composites as pneumatic actuators", *Advanced functional materials*, 2012, vol 22, no 7, pp. 1376-1384.

[15] Nasab A M, Sabzehzar A, Tatari M, et al. "A Soft Gripper with Rigidity Tunable Elastomer Strips as Ligaments", *Soft robotics*, 2017, vol 4, no 4, pp. 411-420.

[16] Hao Y, Wang T, Wen L. "A programmable mechanical freedom and variable stiffness soft actuator with low melting point alloy", in *International conference on intelligent robotics and applications*, Springer, Cham, 2017, pp. 151-161.

[17] Yang Y, Chen Y, Li Y, et al. "Bioinspired robotic fingers based on pneumatic actuator and 3D printing of smart material", *Soft robotics*, 2017, vol 4, no 2, pp. 147-162.

[18] Wang W, Ahn S H. "Shape Memory Alloy-Based Soft Gripper with Variable Stiffness for Compliant and Effective Grasping", *Soft robotics*, 2017, vol 4, no 4, pp. 379-389.

[19] Zhao H, O'Brien K, Li S, et al. "Optoelectronically innervated soft prosthetic hand via stretchable optical waveguides", *Science Robotics*, 2016, vol 1, no 1, pp. eaai7529.

[20] Tavakoli M, Rocha R, Osorio L, et al. "Carbon doped PDMS: Conductance stability over time and implications for additive manufacturing of stretchable electronics", *Journal of Micromechanics and Microengineering*, 2017, vol 27, no 3, pp. 035010.

[21] Truby R L, Wehner M, Grosskopf A K, et al. "Soft somatosensitive actuators via embedded 3D printing", *Advanced Materials*, 2018, vol 30, no 15, pp. 1706383.

[22] Chossat J B, Park Y L, Wood R J, et al. "A soft strain sensor based on ionic and metal liquids", *IEEE Sensors Journal*, 2013, vol 13, no 9, pp. 3405-3414.

[23] Vogt D M, Park Y L, Wood R J. "Design and characterization of a soft multi-axis force sensor using embedded microfluidic channels", *IEEE Sensors Journal*, 2013, vol 13, no 10, pp. 4056-4064.

[24] Chossat J B, Tao Y, Duchaine V, et al. "Wearable soft artificial skin for hand motion detection with embedded microfluidic strain sensing", in *Robotics and Automation (ICRA), 2015 IEEE International Conference on. IEEE*, 2015, pp. 2568-2573.

[25] Webster III R J, Jones B A. "Design and kinematic modeling of constant curvature continuum robots: A review", *The International Journal of Robotics Research*, 2010, vol 29, no 13, pp. 1661-1683.

[26] Morrow J, Shin H S, Phillips-Grafflin C, et al. "Improving Soft Pneumatic Actuator fingers through integration of soft sensors, position and force control, and rigid fingernails", in *Robotics and Automation (ICRA), 2015 IEEE International Conference on. IEEE*, 2016, pp. 5024-5031.

[27] Park Y L, Majidi C, Kramer R, et al. "Hyperelastic pressure sensing with a liquid-embedded elastomer", *Journal of Micromechanics and Microengineering*, 2010, vol 20, no 12, pp. 125029.

[28] Rousseau I A, Xie T. Shape memory epoxy: composition, structure, properties and shape memory performances[J]. Journal of Materials Chemistry, 2010, 20(17): 3431-3441.